Wave propagation in random multi-scale media

Application to quantitative ultrasound imaging

Josselin Garnier [1], Laure Giovangigli [2], Quentin Goepfert [1,2],
Pierre Millien [3], Emile Parolin [4].

[1]CMAP, CNRS, Ecole Polytechnique, Institut Polytechnique de Paris
[2]POEMS, CNRS, Inria, ENSTA Paris, Institut Polytechnique de Paris
[3]Institut Langevin, ESPCI Paris, PSL University, CNRS
[4]Alpines, Inria, LJLL, Sorbonne Université

March 19, 2025.
Journée onde Sud-Ouest

Ultrasound imaging in soft tissues

· Technical progress in sensors manufacturing over the last decades and access to extensive computational resources imply that the fidelity of the image relies on the reconstruction algorithm and the underlying mathematical model.

· Conventional ultrasound imaging algorithms rely on the assumption that the speed of sound is constant in the medium.

Can we go beyond this limitation?

Ultrasound imaging in soft tissues

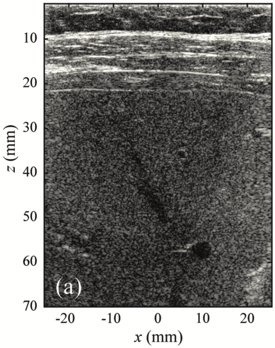

In-vivo image of a human liver [1]

- In soft tissues, the measured echoes come from numerous weakly contrasted unresolved scatterers.
- State of the art models
  - produce stable solutions w.r.t. the sizes and positions of the scatterers
  - see their performance deteriorate when the number of scatterers increases.
  - do not account for the change of effective properties due to the presence of scatterers.

Ultrasound imaging in soft tissues

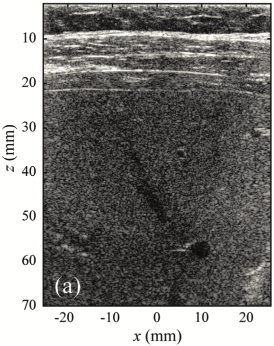

In-vivo image of a human liver [1]

· In soft tissues, the measured echoes come from numerous weakly contrasted unresolved scatterers.

· We aim at providing a mathematical framework for wave propagation in random multi-scale media.

> First goal: Derive a quantitative asymptotic expansion of the measured field w.r.t. the size of the scatterers using stochastic homogenization.

[1] W. Lambert, Matrix approach for ultrasound imaging and quantification, PhD thesis (2020).

Quantitative medical ultrasound imaging

Second goal: justify mathematically the estimators of the effective speed of sound in biological tissues introduced by A. Aubry [2]

- Motivations
  - An incorrect speed c in the algorithm leads to a distorted image.
  - The speed of sound is a quantitative biomarker that can be used for diagnosis (breast cancer, hepatic steatosis...).

[2] F. Bureau, Multi-dimensional analysis of the reflection matrix for quantitative ultrasound imaging, PhD thesis (2023).

Presentation of the model

· We illuminate a smooth bounded medium $D \subset \mathbb{R}^d$ with an incident wave u^i with wave number k.

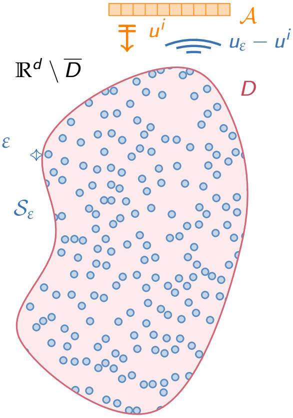

Schema of the model

· In D lies a set of small randomly distributed inclusions $\mathcal{S}_\varepsilon := (S_j^\varepsilon)_{j \in [|1, N_\varepsilon]}$ of size $\varepsilon << k^{-1}$. Typically $N_\varepsilon \sim \varepsilon^{-d}$.

· The medium parameters in D are given by

$$a_\varepsilon := a_m + \sum_{j=1}^{N_\varepsilon} (a_j - a_m) \mathbb{1}_{S_j^\varepsilon},$$

$$n_\varepsilon := n_m + \sum_{j=1}^{N_\varepsilon} (n_j - n_m) \mathbb{1}_{S_j^\varepsilon}.$$

where $a_m, a_j \in \mathcal{M}_d(\mathbb{R})$ are uniformly elliptic and $n_m, n_j \in (n_-, n_+)$ with $n_- > 0$.

· The free space $\mathbb{R}^d \setminus \overline{D}$ is homogeneous with parameters I and 1.

Structure of the presentation

1. Scattered wavefield in the stochastic homogenization regime
   - Effective model
   - First-order asymptotic expansion
   - Numerical simulations
2. Speed of sound estimation
   - Analysis of the point spread function in the paraxial regime
   - Estimation of the effective speed of sound in tissue-mimicking media

Structure of the presentation

1. Scattered wavefield in the stochastic homogenization regime
   - Effective model
   - First-order asymptotic expansion
   - Numerical simulations

2. Speed of sound estimation
   - Analysis of the point spread function in the paraxial regime
   - Estimation of the effective speed of sound in tissue-mimicking media

Structure of the presentation

1. Scattered wavefield in the stochastic homogenization regime
   - Effective model
   - First-order asymptotic expansion
   - Numerical simulations

2. Speed of sound estimation
   - Analysis of the point spread function in the paraxial regime
   - Estimation of the effective speed of sound in tissue-mimicking media

Equation verified by the wavefield u_ε

- A.s. the total wavefield u_ε is the unique solution in $H^1_{loc}(\mathbb{R}^d)$ of

$$\left|\begin{array}{l} -\nabla\cdot(I+(a_\varepsilon-I)\chi_D)\nabla u_\varepsilon - k^2(1+(n_\varepsilon-1)\chi_D)u_\varepsilon = 0 \text{ in } \mathbb{R}^d, \\ u_\varepsilon - u^i \text{ verifies Sommerfeld radiation condition.} \end{array}\right.$$

Equation verified by the wavefield u_ε

· Let $B_R \supset \bar{D}$ be the ball of radius R and $\Lambda : H^{\frac{1}{2}}(\partial B_R) \to H^{-\frac{1}{2}}(\partial B_R)$ be the DtN operator associated to $-\Delta u - k^2 u = 0$ + Sommerfeld r.c..

We consider u_ε the unique solution in $H^1(B_R)$ to

$$\left| \begin{array}{ll} -\nabla \cdot (I + (a_\varepsilon - I)\chi_D)\nabla u_\varepsilon - k^2(1 + (n_\varepsilon - 1)\chi_D)u_\varepsilon = 0 & \text{in } B_R, \\ \partial_n(u_\varepsilon - u^i) = \Lambda(u_\varepsilon - u^i) & \text{on } \partial B_R. \end{array} \right.$$

Equation verified by the wavefield u_ε

· Let $B_R \supset \bar{D}$ be the ball of radius R and $\Lambda : H^{\frac{1}{2}}(\partial B_R) \to H^{-\frac{1}{2}}(\partial B_R)$ be the DtN operator associated to $-\Delta u - k^2 u = 0$ + Sommerfeld r.c..

We consider u_ε the unique solution in $H^1(B_R)$ to

$$\left| \begin{array}{ll} -\nabla \cdot (I + (a_\varepsilon - I)\chi_D)\nabla u_\varepsilon - k^2(1 + (n_\varepsilon - 1)\chi_D)u_\varepsilon = 0 & \text{in } B_R, \\ \partial_n(u_\varepsilon - u^i) = \Lambda(u_\varepsilon - u^i) & \text{on } \partial B_R. \end{array} \right.$$

· We suppose that the sesquilinear form associated to (1) is coercive.

There exists C_R independent of ε and the realization such that

$$\|u_\varepsilon\|_{H^1(B_R)} \leq C_R \|u_i\|_{H^1(D)}.$$

Random setting

· Let $\{\boldsymbol{x}_j\}_j$ denote the point process corresponding to the centers of the inclusions. Let S_j be the inclusion with size 1 centered at $\boldsymbol{x}_j$.

· We suppose that $\{\boldsymbol{x}_j\}_j$ is stationary, *i.e.* its distribution law $\mathbb{P}$ is independent of the spatial variable.

· Let $\mathcal{S} := \bigcup_{j\in\mathbb{N}} S_j$ be the set of inclusions in $\mathbb{R}^d$. We define for $\boldsymbol{x} \in \mathbb{R}^d$

$$a(\boldsymbol{x}) = a_m + \sum_{j\in\mathbb{N}} (a_j - a_m)\mathbb{1}_{S_j}(\boldsymbol{x}),$$

$$\text{and} \quad n(\boldsymbol{x}) = n_m + \sum_{j\in\mathbb{N}} (n_j - n_m)\mathbb{1}_{S_j}(\boldsymbol{x}).$$

Then $\mathcal{S}_\varepsilon := \varepsilon\mathcal{S} \cap D$, $a_\varepsilon(\cdot) := a(\frac{\cdot}{\varepsilon})$ and $n_\varepsilon(\cdot) := n(\frac{\cdot}{\varepsilon})$.

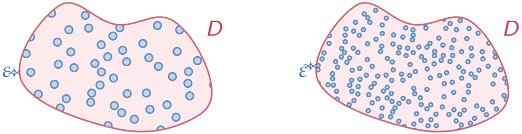

Schema of the medium for different ε.

Definitions

- Let Ω be the set of point processes in $\mathbb{R}^d$.
- We introduce the translation operator $\tau : \Omega \times \mathbb{R}^d \to \Omega$

$$\forall \varpi \in \Omega, \forall \boldsymbol{x} \in \mathbb{R}^d,\ \tau(\varpi, \boldsymbol{x}) = \varpi' \text{ s.t. } \forall j \in \mathbb{N},\ \boldsymbol{x}_j^{\varpi'} = \boldsymbol{x}_j^{\varpi} + \boldsymbol{x}.$$

The action $(\tau_{\boldsymbol{x}})_{\boldsymbol{x} \in \mathbb{R}^d}$ preserves the measure $\mathbb{P}$.

Definition : $f : \mathbb{R}^d \times \Omega \to \mathbb{R}^p$ is said to be stationary w.r.t τ iff

$$\forall \boldsymbol{x}, \boldsymbol{y} \in \mathbb{R}^d, \forall \text{ a.e. } \varpi \in \Omega,\ f^{\varpi}(\boldsymbol{x} + \boldsymbol{y}) = f^{\tau_{\boldsymbol{y}}\varpi}(\boldsymbol{x}).$$

We suppose moreover that the action $(\tau_{\boldsymbol{x}})_{\boldsymbol{x} \in \mathbb{R}^d}$ is ergodic.

Theorem : Birkhoff ergodic theorem

Let $f \in L^1_{loc}(\mathbb{R}^d, L^1(\Omega))$ be a stationary process w.r.t. an ergodic action. Then a.s. and in $L^1(\Omega)$

$$\forall x \in \mathbb{R}^d, \quad \frac{1}{|B_R|} \int_{B_R} f(\boldsymbol{y} + \boldsymbol{x})\, d\boldsymbol{y} \xrightarrow[R \uparrow \infty]{} \mathbb{E}(f).$$

Coherent wave

- A.s. for all ball B_R, u_ε converges weakly in $H^1(B_R)$ to $u^\star$ solution of

$$\left|\begin{array}{ll} -\nabla \cdot (I + (a^\star - I)\chi_D)\nabla u^\star - k^2(1 + (n^\star - 1)\chi_D)u^\star = 0 & \text{in } B_R, \\ \partial_n(u^\star - u^i) = \Lambda(u^\star - u^i) & \text{on } \partial B_R. \end{array}\right.$$

where the homogenized coefficients $a^\star$ and $n^\star$ are defined as

$$\forall i, j \in [|1, d|], a^\star_{i,j} = \mathbb{E}[e_i \cdot a(e_j + \nabla \phi_j)], \text{ and } n^\star = \mathbb{E}[n].$$

ϕ_j is the standard corrector in stochastic homogenization.

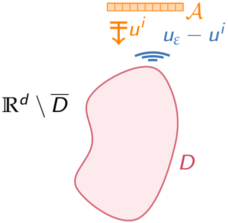

Figure: Homogenized model

Corrector equation

- For $i \in [|1, d|]$, there exists a unique ϕ_i (up to a random constant) s.t.
  - (a) a.s. $\phi_i(\cdot) \in H^1_{loc}(\mathbb{R}^d)$ is solution of

$$\boxed{-\nabla \cdot a(y)(\nabla \phi_i(y) + e_i) = 0 \quad \text{in}\, \mathcal{D}'(\mathbb{R}^d),}$$

  - (b) $\nabla \phi_i \in L^2_{loc}(\mathbb{R}^d, L^2(\Omega))$, $\nabla \phi_i$ is stationary and $\mathbb{E}(\nabla \phi_i) = 0$.

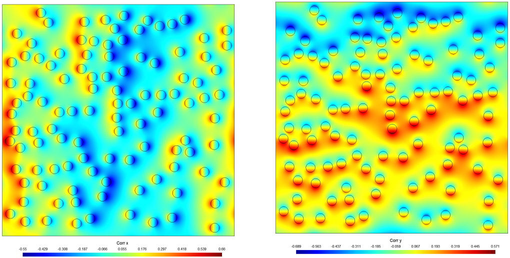

Figure: Numerical simulations of the correctors (left: ϕ_1, right: ϕ_2)

Structure of the presentation

1. Scattered wavefield in the stochastic homogenization regime
   Effective model
   First-order asymptotic expansion
   Numerical simulations

2. Speed of sound estimation
   Analysis of the point spread function in the paraxial regime
   Estimation of the effective speed of sound in tissue-mimicking media

Corrector bounds

· In order to establish error estimates, we add a quantitative mixing assumption $\mathcal{H}_m$ on $\mathcal{S}$ [3]. $\mathcal{H}_m$ implies in particular that its covariance function is integrable.

Theorem: Corrector bounds [3]

Under $\mathcal{H}_m$, there exists an a.s. finite random field $\boldsymbol{x} \mapsto \mathcal{C}(\boldsymbol{x})$ with exponential moments s.t.

$$\forall \boldsymbol{x} \in \mathbb{R}^d, \quad \left(\fint_{\square_{\boldsymbol{x}}} |\phi|^2 \right)^{\frac{1}{2}} \leq \mathcal{C}(\boldsymbol{x}) \mu_d(|\boldsymbol{x}|),$$

where $\square_{\boldsymbol{x}} := [-\frac{1}{2} + \boldsymbol{x}, \frac{1}{2} + \boldsymbol{x}]^d$ and

$$\mu_d(\cdot) := \begin{cases} |\log(2+\cdot)|^{\frac{1}{2}} & \text{if } d = 2, \\ 1 & \text{if } d = 3. \end{cases}$$

[3] A. Gloria, S. Neukamm, F. Otto (2019), S. Armstrong, T. Kuusi, JC. Mourrat (2019)

First-order two-scale expansion in D

- For $\boldsymbol{x} \in D$, we define $u_1(\boldsymbol{x}) := \sum_{i=1}^{d} \phi_i(\frac{\boldsymbol{x}}{\varepsilon})\partial_i u^\star(\boldsymbol{x})$.

Theorem: Error estimates

Under a quantitative mixing assumption on a and n, for all ball B_R

$$\mathbb{E}[||u_\varepsilon - u^\star||^2_{L^2(B_R)}]^{1/2} \lesssim \varepsilon\mu_d\left(\frac{1}{\varepsilon}\right),$$

$$\mathbb{E}[||u_\varepsilon - u^\star - \varepsilon u_1||^2_{H^1(D)}]^{1/2} \lesssim \varepsilon^{\frac{1}{2}}\mu_d\left(\frac{1}{\varepsilon}\right)^{\frac{1}{2}}.$$

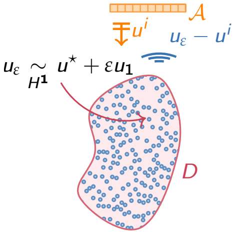

This result was known for Laplace Dirichlet or Neumann problems [4], but not for the Helmholtz transmission problem. It required to introduce the associated boundary correctors and quantify them.

[4] Quantitative stochastic homogenization and large-scale regularity, S. Armstrong, T. Kuusi, JC. Mourrat (2019)

Main steps of the proof

- We write the problem verified in B_R by $v_\varepsilon := u_\varepsilon - u^\star - \varepsilon u_1 \mathbb{1}_D$.

- Let θ_ε be the boundary corrector s.t. $v_\varepsilon - \theta_\varepsilon$ verifies the transmission conditions on ∂D. $\theta_\varepsilon \in H^1(B_R \setminus \overline{D}) \times H^1(D)$ is the a.s. solution of:

$$\begin{cases} -\Delta\theta_\varepsilon - k^2\theta_\varepsilon = 0 & \text{in } B_R \setminus \overline{D}, \\ -\nabla \cdot a_\varepsilon \nabla\theta_\varepsilon - k^2 n_\varepsilon \theta_\varepsilon = 0 & \text{in } D, \\ \theta_\varepsilon^- - \theta_\varepsilon^+ = \varepsilon u_1 & \text{on } \partial D, \\ \partial_n \theta_\varepsilon^- - a_\varepsilon \partial_n \theta_\varepsilon^+ \cdot \nu = \varepsilon F_\varepsilon & \text{on } \partial D, \\ \partial_n \theta_\varepsilon = \Lambda(\theta_\varepsilon) & \text{on } \partial B_R, \end{cases}$$

with F_ε that depends on correctors and $u^\star$.

- Related works on boundary layer correctors:
  - Periodic setting: Gérard-Varet, Masmoudi (2011-2012) - Prange (2013) - Fliss, Joly, Vinoles (2016) - Cakoni, Guzina, Moskow (2016) - Beneteau, Claeys, Fliss (2021).
  - Stochastic setting: Armstrong, Kuusi, Mourrat (2019) - Josien, Raithel (2021).

Main steps of the proof

· We write the problem verified in B_R by $v_\varepsilon := u_\varepsilon - u^\star - \varepsilon u_1 \mathbb{1}_D$.

· Let θ_ε be the boundary corrector s.t. $v_\varepsilon - \theta_\varepsilon$ verifies the transmission conditions on ∂D. $\theta_\varepsilon \in H^1(B_R \setminus \overline{D}) \times H^1(D)$ is the a.s. solution of:

$$\begin{cases} -\Delta\theta_\varepsilon - k^2\theta_\varepsilon = 0 & \text{in } B_R \setminus \overline{D}, \\ -\nabla \cdot a_\varepsilon \nabla\theta_\varepsilon - k^2 n_\varepsilon \theta_\varepsilon = 0 & \text{in } D, \\ \theta_\varepsilon^- - \theta_\varepsilon^+ = \varepsilon u_1 & \text{on } \partial D, \\ \partial_n \theta_\varepsilon^- - a_\varepsilon \partial_n \theta_\varepsilon^+ \cdot \nu = \varepsilon F_\varepsilon & \text{on } \partial D, \\ \partial_n \theta_\varepsilon = \Lambda(\theta_\varepsilon) & \text{on } \partial B_R, \end{cases}$$

with F_ε that depends on correctors and $u^\star$.

· We estimate the H^1-norm of $v_\varepsilon - \theta_\varepsilon$ thanks to the correctors bounds.

· We estimate the L^2- and H^1- norms of θ_ε which verifies a similar problem as u_ε with oscillatory data on ∂D.

A new integral representation for the total field

- For $\boldsymbol{z} \in B_R \setminus \overline{D}$, u_ε verifies

$$u_\varepsilon(\boldsymbol{z}) = u^\star(\boldsymbol{z}) \quad + \int_D (a^\star - a_\varepsilon)\nabla u_\varepsilon \cdot \nabla G^\star(\cdot,\boldsymbol{z}) + k^2 \int_D (n_\varepsilon - n^\star) u_\varepsilon G^\star(\cdot,\boldsymbol{z}).$$

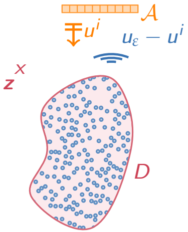

where $G^\star(\cdot,\boldsymbol{y})$ is the Green function associated to the homogenized problem, *i.e.* the unique solution for $\boldsymbol{y} \in B_R$ of

$$\left| \begin{array}{ll} -\nabla\cdot(I + (a^\star - I)\chi_D)\nabla G^\star - k^2(1 + (n^\star - 1)\chi_D)G^\star = \delta_{\boldsymbol{y}} & \text{in } B_R, \\ \partial_n G^\star = \Lambda G^\star & \text{on } \partial B_R. \end{array} \right.$$

Asymptotic expansion of of the outer field

Theorem:

Let $\alpha > 0$. Under $\mathcal{H}_m$, for $\boldsymbol{z} \in B_R \setminus \overline{(1+\alpha)D}$

$$\mathrm{Var}\left[|u_\varepsilon(\boldsymbol{z}) - u^\star(\boldsymbol{z}) - \mathcal{U}_1(\boldsymbol{z})|\right]^{\frac{1}{2}} \lesssim \varepsilon^{\frac{d+1}{2}} \mu_d\left(\frac{1}{\varepsilon}\right)^{\frac{1}{2}},$$

where

$$\mathcal{U}_1 := \int_D (a^\star - a_\varepsilon(\boldsymbol{x}))\left[\nabla u^\star(\boldsymbol{x}) + \nabla_y u_1\left(\boldsymbol{x}, \frac{\boldsymbol{x}}{\varepsilon}\right)\right] \cdot \nabla G^\star(\boldsymbol{x}, \cdot) d\boldsymbol{x}$$
$$-k^2 \int_D (n^\star - n_\varepsilon(\boldsymbol{x})) u^\star(\boldsymbol{x}) G^\star(\boldsymbol{x}, \cdot) d\boldsymbol{x}.$$

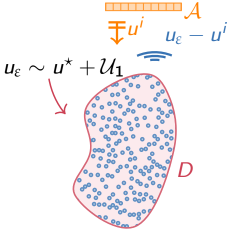

The proof requires to quantify the fluctuations of the two-scale error.

Related work: M. Duerinckx, A. Gloria and F. Otto (2020)

Structure of the presentation

1. Scattered wavefield in the stochastic homogenization regime
   - Effective model
   - First-order asymptotic expansion
   - Numerical simulations
2. Speed of sound estimation
   - Analysis of the point spread function in the paraxial regime
   - Estimation of the effective speed of sound in tissue-mimicking media

The medium

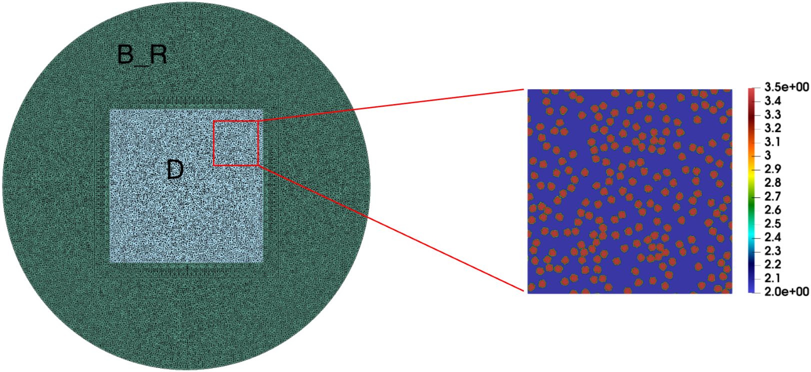

Figure: Mesh of the domain and realization of a_ε.

Reference solution u_ε

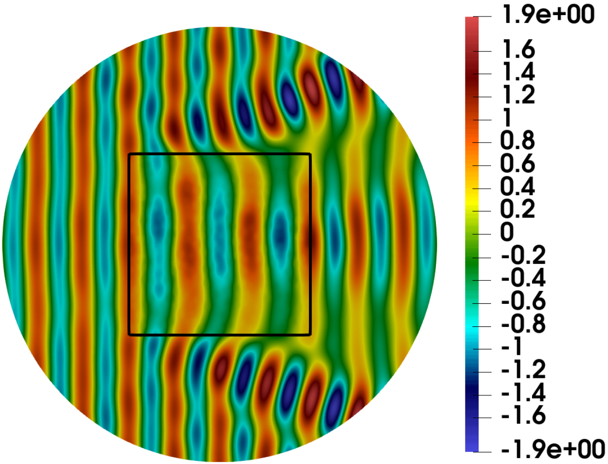

Figure: Simulation of the scattered field u_ε

Homogenized solution $u^\star$

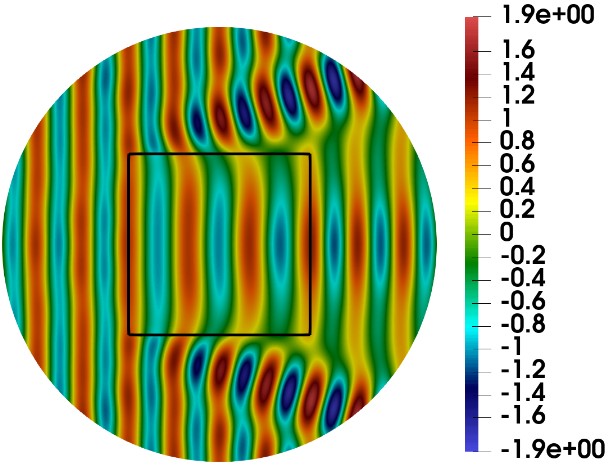

Figure: Simulation of the homogenized field $u^\star$

Error field $u_\varepsilon - u^\star$

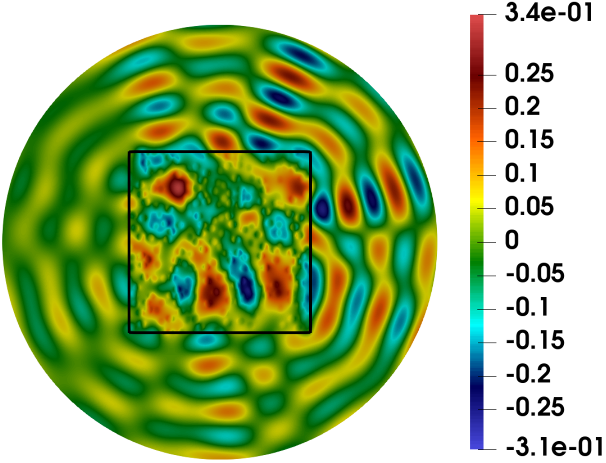

Figure: Simulation of the error field $u_\varepsilon - u^\star$

First-order expansion term $\mathcal{U}_1$

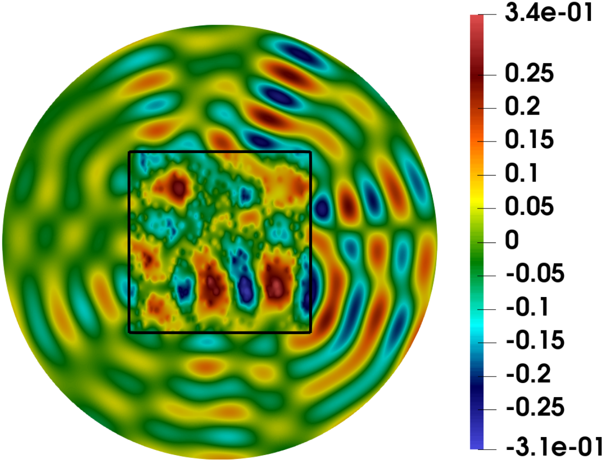

Figure: Simulation of the approximated scattered field

Convergence rates

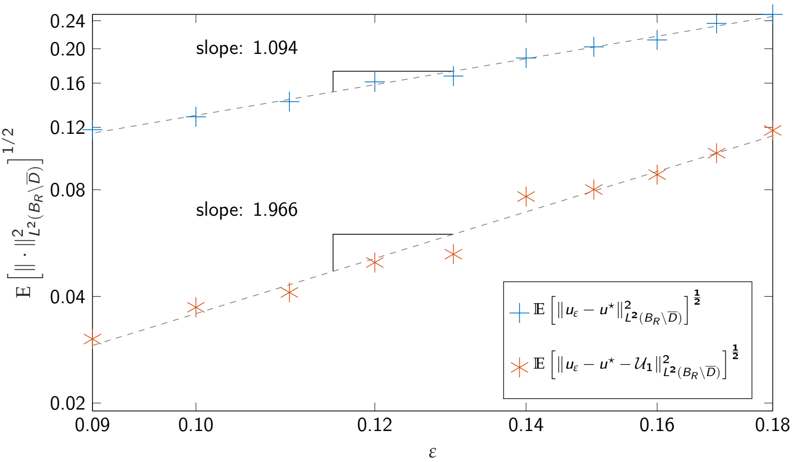

Figure: Convergence rates for the norm $\mathbb{E}[||\cdot||^2_{L^2(B_R\setminus\bar{D})}]^{1/2}$

Structure of the presentation

1. Scattered wavefield in the stochastic homogenization regime
   - Effective model
   - First-order asymptotic expansion
   - Numerical simulations

2. Speed of sound estimation
   - Analysis of the point spread function in the paraxial regime
   - Estimation of the effective speed of sound in tissue-mimicking media

Principle of ultrasound imaging

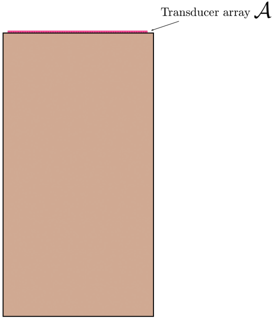

Simulation
of an US experiment

Let $c^\star$ be the effective speed of sound in the medium D.

· For a frequency $\omega \in \mathcal{B}$, an incident wave $u^i(\boldsymbol{x}_e, \cdot, \omega)$ is emitted in D from $\boldsymbol{x}_e \in \mathcal{A}$ with wave number $\frac{\omega}{c^\star}$.

· The scattered field $u^s_\varepsilon(\boldsymbol{x}_e, \boldsymbol{x}_r, \omega,) := u_\varepsilon - u^i$ is recorded by the transducers at $\boldsymbol{x}_r \in \mathcal{A}$.

· The image at $\boldsymbol{z}$ is computed by Kirchhoff migration with backpropagation speed c

$$\mathcal{I}^c(\boldsymbol{z}) = \int_{\mathcal{B}\times\mathcal{A}\times\mathcal{A}} \overline{u}^s_\varepsilon(\boldsymbol{x}_e, \boldsymbol{x}_r, \omega) G^{\frac{\omega}{c}}(\boldsymbol{x}_e, \boldsymbol{z}) G^{\frac{\omega}{c}}(\boldsymbol{z}, \boldsymbol{x}_r) d\boldsymbol{x}_e d\boldsymbol{x}_r d\omega,$$

where G^k is the outgoing Green's function of Helmholtz equation with wavenumber k.

Principle of ultrasound imaging

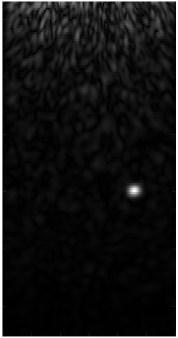

Computed image

Let $c^\star$ be the effective speed of sound in the medium D.

· For a frequency $\omega \in \mathcal{B}$, an incident wave $u^i(\boldsymbol{x}_e, \cdot, \omega)$ is emitted in D from $\boldsymbol{x}_e \in \mathcal{A}$ with wave number $\frac{\omega}{c^\star}$.

· The scattered field $u^s_\varepsilon(\boldsymbol{x}_e, \boldsymbol{x}_r, \omega)$ is recorded by the transducers at $\boldsymbol{x}_r \in \mathcal{A}$.

· The image at $\boldsymbol{z}$ is computed by Kirchhoff migration with backpropagation speed c

$$\mathcal{I}^c(\boldsymbol{z}) = \int_{\mathcal{B}\times\mathcal{A}\times\mathcal{A}} \overline{u}^s_\varepsilon(\boldsymbol{x}_e, \boldsymbol{x}_r, \omega) G^{\frac{\omega}{c}}(\boldsymbol{x}_e, \boldsymbol{z}) G^{\frac{\omega}{c}}(\boldsymbol{z}, \boldsymbol{x}_r) d\boldsymbol{x}_e d\boldsymbol{x}_r d\omega.$$

Goal: Estimate $c^\star$ from the measurements u^s_ε.

State of the art

- Full waveform inversion: C. Li, G. S. Sandhu, O. Roy, N. Duric, V. Allada, and S. Schmidt (2014), S. Bernard, V. Monteiller, D. Komatitsch, and P. Lasaygues (2017), L. Guasch, O. C. Agudo, M.-X. Tang, P. Nachev, and M. Warner (2020), F. Faucher and O. Scherzer (2022)

- On the physics side
  - Compounding methods (CUTE) M. Jaeger, G. Held, S. Peeters, S. Preisser, M. Grünig, and M. Frenz (2015), Goksel (2021)
  - Focusing methods Ogawa (2019), A. Aubry (2023)

Expression of the imaging function

- We make two simplifications on the medium parameters in D:
  - constant density, *i.e.* $a_\varepsilon := 1$,
  - match between the homogenized and outer media $(u^\star = u^i)$, *i.e.* $n^\star = 1$.
- The results of the previous section give for $\boldsymbol{z} \in D'$

$$\boxed{\mathcal{I}^c(\boldsymbol{z}) = \int_D (n_\varepsilon(\boldsymbol{y}) - n^\star) F^c(\boldsymbol{z}, \boldsymbol{y}) \mathrm{d}\boldsymbol{y}.}$$

where the kernel $F^c : D' \times D \mapsto \mathbb{C}$ is defined by

$$\boxed{F^c(\boldsymbol{z}, \boldsymbol{y}) = \int_{\mathcal{B}} \left(\frac{\omega}{c^\star}\right)^2 \left(\int_{\mathcal{A}} G^{\frac{\omega}{c}}(\boldsymbol{y}, \boldsymbol{x}_r) G^\star(\boldsymbol{y}, \boldsymbol{x}_r) \mathrm{d}\boldsymbol{x}_r\right)^2 \mathrm{d}\omega.}$$

F^c is the point spread function, *i.e.* the imaging function at $\boldsymbol{z}$ when a point reflector lies at $\boldsymbol{y}$.

Structure of the presentation

1. Scattered wavefield in the stochastic homogenization regime
   - Effective model
   - First-order asymptotic expansion
   - Numerical simulations

2. Speed of sound estimation
   - Analysis of the point spread function in the paraxial regime
   - Estimation of the effective speed of sound in tissue-mimicking media

Paraxial asymptotic regime

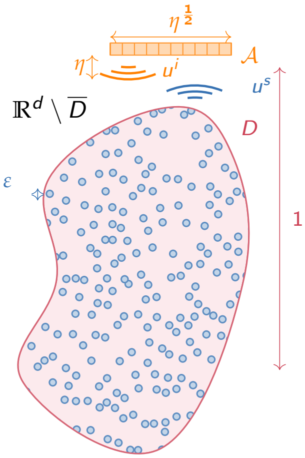

Schema of the model

- Typical values for the parameters:
  - Bandwidth: $\mathcal{B} \sim [2, 4]$ MHz,
  - Speed of sound: $c^\star \sim [1400, 1600]$ m·s^{-1}

    ⟶ Wavelength: $\lambda \sim 1$ mm
  - Size of D: $5 \times [10, 15]$ cm
  - Size of $\mathcal{A}$: $a \sim 4$cm.
  - Size of the scatterers: $\varepsilon \sim 5\mu$m

$$\varepsilon \ll \frac{c^\star}{\omega} \ll a \ll \mathrm{diam}(D).$$

Paraxial asymptotic regime

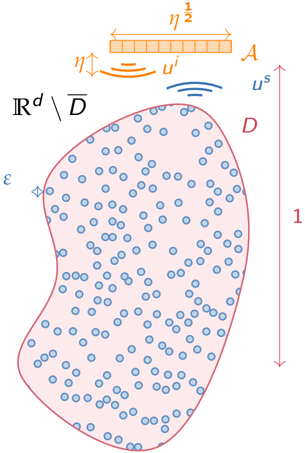

Schema of the model

- We consider the paraxial asymptotic regime:
  - Bandwidth: $\mathcal{B} := \dfrac{\mathcal{B}_0}{\eta}$ with
  $$\mathcal{B}_0 := [\omega_0 - \frac{B}{2}, \omega_0 + \frac{B}{2}],$$
  - Transducers array:
  $$\mathcal{A} := \eta^{\frac{1}{2}} \mathcal{A}_0 := \eta^{\frac{1}{2}} [-\frac{a_0}{2}, \frac{a_0}{2}]^{d-1},$$
  - Scatterers: $\varepsilon := o(\eta)$,
  - Point in the paraxial regime:
  $$\boldsymbol{y} := (\boldsymbol{y}_\eta^{\perp}, y^{\shortparallel}) := (\eta^{\frac{1}{2}} \boldsymbol{y}^{\perp}, y^{\shortparallel}).$$

where $\eta \ll 1$ is a small scaling parameter.

Point spread function for different backpropagation speeds

- $F^c(\cdot, \boldsymbol{y}_0)$ for different backpropagation speeds $c = \nu c^\star$ and $\boldsymbol{y}_0 \in D$

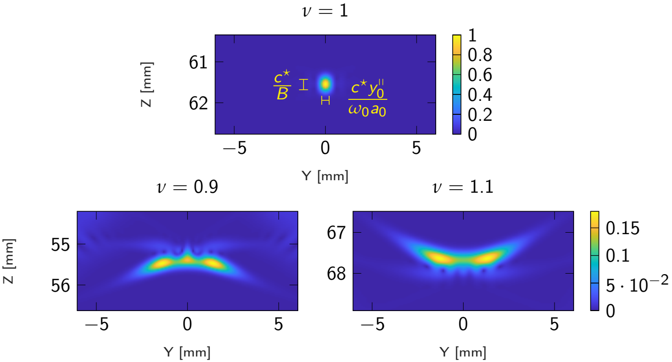

- The shape and position of the focal spot on the image and the max amplitude are altered by a mismatch.

Point spread function in the paraxial regime

- For $\boldsymbol{y}_0 := (\eta^{\frac{1}{2}} y_0^{\perp}, y_0^{||})$, the focal spot on the image is centered at:

$$\varphi_c(\boldsymbol{y}_0) := \left(\left(\tfrac{c}{c^\star}\right)^2 \eta^{\frac{1}{2}} y_0^{\perp}, \tfrac{c}{c^\star} y_0^{||} \right).$$

Theorem : Narrowband PSF in the paraxial regime

Let $\boldsymbol{z} := \varphi_c(\boldsymbol{y}_0) + \left(\eta^{\frac{1}{2}} \left(\tfrac{c}{c^\star}\right)^2 \zeta_1, \eta \tfrac{c}{c^\star} \zeta_2 \right)$ with $\zeta := (\zeta_1, \zeta_2) \in \mathbb{R}^2$.

$$F^c(\boldsymbol{z}, \boldsymbol{y}_0) \sim \exp\left(\frac{2i\omega_0}{c^\star} \left(\zeta_2 - \frac{|y_0^{\perp}|^2 - (\frac{c}{c^\star})^2 |y_0^{\perp} + \zeta_1|^2}{2y_0^{||}} \right) \right)$$
$$\operatorname{sinc}\left(\frac{B}{c^\star} \zeta_2 \right) \mathcal{G}\left(\frac{a_0 \omega_0}{y_0^{||} c^\star} \zeta_1, \frac{a_0^2 \omega_0}{y_0^{||} c^\star} \left(\left(\frac{c^\star}{c} \right)^2 - 1 \right) \right)^2,$$

where $\mathcal{G}$ is the peak function defined by:

$$\mathcal{G}(\xi_1, \xi_2) := \frac{1}{|\mathcal{A}_0|} \int_{\mathcal{A}_0} \exp\left(-i x_e \cdot \xi_1 + i \frac{|x_e|^2}{2} \xi_2 \right) d\sigma(x_e).$$

Point spread function in the paraxial regime

- For $\boldsymbol{y_0} := (\eta^{\frac{1}{2}} y_0^{\perp}, y_0^{||})$, the focal spot on the image is centered at:

$$\boxed{\varphi_c(\boldsymbol{y_0}) := \left(\left(\tfrac{c}{c^\star}\right)^2 \eta^{\frac{1}{2}} y_0^{\perp}, \tfrac{c}{c^\star} y_0^{||} \right).}$$

Theorem : Narrowband PSF in the paraxial regime

Let $\boldsymbol{z} := \varphi_c(\boldsymbol{y_0}) + \left(\eta^{\frac{1}{2}} \left(\tfrac{c}{c^\star}\right)^2 \zeta_1, \eta \tfrac{c}{c^\star} \zeta_2 \right)$ with $\zeta := (\zeta_1, \zeta_2) \in \mathbb{R}^2$.

$$F^c(\boldsymbol{z}, \boldsymbol{y_0}) \sim \exp\left(\frac{2i\omega_0}{c^\star} \left(\zeta_2 - \frac{|y_0^{\perp}|^2 - (\frac{c}{c^\star})^2 |y_0^{\perp} + \zeta_1|^2}{2 y_0^{||}} \right) \right)$$
$$\boxed{\operatorname{sinc}\left(\frac{B}{c^\star} \zeta_2 \right)} \mathcal{G}\left(\boxed{\frac{a_0 \omega_0}{y_0^{||} c^\star} \zeta_1}, \frac{a_0^2 \omega_0}{y_0^{||} c^\star} \left(\left(\frac{c^\star}{c} \right)^2 - 1 \right) \right)^2,$$

where $\mathcal{G}$ is the peak function defined by:

$$\mathcal{G}(\xi_1, \xi_2) := \frac{1}{|\mathcal{A}_0|} \int_{\mathcal{A}_0} \exp\left(-i x_e \cdot \xi_1 + i \frac{|x_e|^2}{2} \xi_2 \right) d\sigma(x_e).$$

Point spread function in the paraxial regime

- For $\boldsymbol{y}_0 := (\eta^{\frac{1}{2}} y_0^{\perp}, y_0^{||})$, the focal spot on the image is centered at:

$$\boxed{\varphi_c(\boldsymbol{y}_0) := \left(\left(\tfrac{c}{c^\star}\right)^2 \eta^{\frac{1}{2}} y_0^{\perp}, \tfrac{c}{c^\star} y_0^{||} \right).}$$

Theorem : Narrowband PSF in the paraxial regime

Let $\boldsymbol{z} := \varphi_c(\boldsymbol{y}_0) + \left(\eta^{\frac{1}{2}} \left(\tfrac{c}{c^\star}\right)^2 \zeta_1, \eta \tfrac{c}{c^\star} \zeta_2 \right)$ with $\zeta := (\zeta_1, \zeta_2) \in \mathbb{R}^2$.

$$F^c(\boldsymbol{z}, \boldsymbol{y}_0) \sim \exp\left(\frac{2i\omega_0}{c^\star} \left(\zeta_2 - \frac{|y_0^{\perp}|^2 - (\frac{c}{c^\star})^2 |y_0^{\perp} + \zeta_1|^2}{2 y_0^{||}} \right) \right) \boxed{\operatorname{sinc}\left(\frac{B}{c^\star} \zeta_2 \right)} \mathcal{G}\left(\boxed{\frac{a_0 \omega_0}{y_0^{||} c^\star} \zeta_1}, \boxed{\frac{a_0^2 \omega_0}{y_0^{||} c^\star} \left(\left(\frac{c^\star}{c} \right)^2 - 1 \right)} \right)^2,$$

where $\mathcal{G}$ is the peak function defined by:

$$\mathcal{G}(\xi_1, \xi_2) := \frac{1}{|\mathcal{A}_0|} \int_{\mathcal{A}_0} \exp\left(-i x_e \cdot \xi_1 + i \frac{|x_e|^2}{2} \xi_2 \right) d\sigma(x_e).$$

Speed of sound estimation

For a given c and $\boldsymbol{y}_0 \in D$, the PSF at the center of the focal spot is

$$F^c(\varphi_c(\boldsymbol{y}_0), \boldsymbol{y}_0) \sim \mathcal{G}\left(0,\ \frac{a_0^2\omega_0}{y_0^{||}c^\star}\left(\left(\frac{c^\star}{c}\right)^2 - 1\right)\right)^2.$$

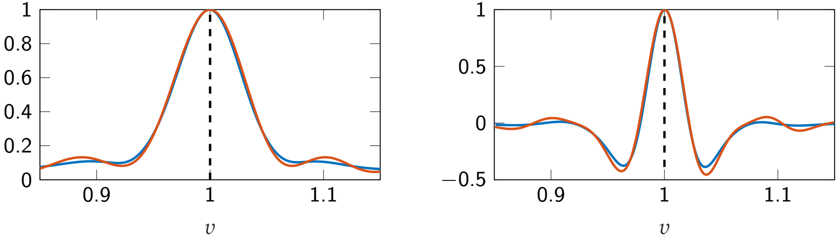

(a) $\hat{c^\star}^{(1)} := \operatorname{argmax}_c |F^c(\varphi_c(\boldsymbol{y}_0), \boldsymbol{y}_0)|$ (b) $\hat{c^\star}^{(2)} := \operatorname{argmax}_c \partial_c \Im[F^c(\varphi_c(\boldsymbol{y}_0), \boldsymbol{y}_0)]$

Figure: Simulation (—) & theoretical (—) estimators of the speed of sound.

1. Scattered wavefield in the stochastic homogenization regime
   - Effective model
   - First-order asymptotic expansion
   - Numerical simulations

2. Speed of sound estimation
   - Analysis of the point spread function in the paraxial regime
   - Estimation of the effective speed of sound in tissue-mimicking media

Virtual guide star

Let $\delta > 0$ be a given threshold and c *not too far* from $c^\star$.

· For $\boldsymbol{y}_0 \in D$, we define the focal spot $\mathcal{D}_\delta(c, \boldsymbol{y}_0)$ on the image D' as

$$\int_{D' \setminus \mathcal{D}_\delta(c, \boldsymbol{y}_0)} |F^c(\boldsymbol{z}, \boldsymbol{y}_0)| \mathrm{d}\boldsymbol{z} \leq \delta \int_{D'} |F^c(\boldsymbol{z}, \boldsymbol{y}_0)| \mathrm{d}\boldsymbol{z}, .$$

$\mathcal{D}_\delta(c, \boldsymbol{y}_0)$ is centered at $\varphi_c(\boldsymbol{y}_0)$.

Virtual guide star

Let $\delta > 0$ be a given threshold and c *not too far* from $c^\star$.

· For $\boldsymbol{y}_0 \in D$, we define the focal spot $\mathcal{D}_\delta(c, \boldsymbol{y}_0)$ on the image D' as

$$\int_{D' \setminus \mathcal{D}_\delta(c, \boldsymbol{y}_0)} |F^c(\boldsymbol{z}, \boldsymbol{y}_0)| \mathrm{d}\boldsymbol{z} \leq \delta \int_{D'} |F^c(\boldsymbol{z}, \boldsymbol{y}_0)| \mathrm{d}\boldsymbol{z}, .$$

$\mathcal{D}_\delta(c, \boldsymbol{y}_0)$ is centered at $\varphi_c(\boldsymbol{y}_0)$.

· For $\boldsymbol{z}_0 \in D'$ we define the dual focal spot $\mathcal{D}'_\delta(c, \boldsymbol{z}_0)$ in the domain D as

$$\int_{D \setminus \mathcal{D}'_\delta(c, \boldsymbol{z}_0)} |F^c(\boldsymbol{z}_0, \boldsymbol{y})| \mathrm{d}\boldsymbol{y} \leq \delta \int_{D} |F^c(\boldsymbol{z}_0, \boldsymbol{y})| \mathrm{d}\boldsymbol{y}.$$

$\mathcal{D}'_\delta(c, \boldsymbol{z}_0)$ is centered at $\varphi_c^{-1}(\boldsymbol{z}_0)$.

Virtual guide star

Let $\delta > 0$ be a given threshold and c *not too far* from $c^\star$.

- For $\boldsymbol{y}_0 \in D$, we define the focal spot $\mathcal{D}_\delta(c, \boldsymbol{y}_0)$ on the image D' as

$$\int_{D' \setminus \mathcal{D}_\delta(c,\boldsymbol{y}_0)} |F^c(\boldsymbol{z}, \boldsymbol{y}_0)| \mathrm{d}\boldsymbol{z} \leq \delta \int_{D'} |F^c(\boldsymbol{z}, \boldsymbol{y}_0)| \mathrm{d}\boldsymbol{z}, .$$

$\mathcal{D}_\delta(c, \boldsymbol{y}_0)$ is centered at $\varphi_c(\boldsymbol{y}_0)$.

- For $\boldsymbol{z}_0 \in D'$ we define the dual focal spot $\mathcal{D}'_\delta(c, \boldsymbol{z}_0)$ in the domain D as

$$\int_{D \setminus \mathcal{D}'_\delta(c,\boldsymbol{z}_0)} |F^c(\boldsymbol{z}_0, \boldsymbol{y})| \mathrm{d}\boldsymbol{y} \leq \delta \int_{D} |F^c(\boldsymbol{z}_0, \boldsymbol{y})| \mathrm{d}\boldsymbol{y}.$$

$\mathcal{D}'_\delta(c, \boldsymbol{z}_0)$ is centered at $\varphi_c^{-1}(\boldsymbol{z}_0)$.

- For $\boldsymbol{z} \in D'$, $\mathcal{I}^c(\boldsymbol{z})$ only depends on the scatterers in $\mathcal{D}'_\delta(c, \boldsymbol{z})$

$$\boxed{\mathcal{I}^c(\boldsymbol{z}) = \int_D (n_\varepsilon(\boldsymbol{y}) - n^\star) F^c(\boldsymbol{z}, \boldsymbol{y}) \mathrm{d}\boldsymbol{y} \sim \int_{\mathcal{D}'_\delta(c,\boldsymbol{z})} (n_\varepsilon(\boldsymbol{y}) - n^\star) F^c(\boldsymbol{z}, \boldsymbol{y}) \mathrm{d}\boldsymbol{y}.}$$

Virtual guide star

Let $\delta > 0$ be a given threshold and c *not too far* from $c^\star$.

- For $\boldsymbol{z} \in D'$, $\mathcal{I}^c(\boldsymbol{z})$ only depends on the scatterers in $\mathcal{D}'_\delta(c, \boldsymbol{z})$

$$\boxed{\mathcal{I}^c(\boldsymbol{z}) = \int_D (n_\varepsilon(\boldsymbol{y}) - n^\star) F^c(\boldsymbol{z}, \boldsymbol{y}) \mathrm{d}\boldsymbol{y} \sim \int_{\mathcal{D}'_\delta(c,\boldsymbol{z})} (n_\varepsilon(\boldsymbol{y}) - n^\star) F^c(\boldsymbol{z}, \boldsymbol{y}) \mathrm{d}\boldsymbol{y}.}$$

- For a fixed $\boldsymbol{z}_0 \in D'$, $c \mapsto \mathcal{I}^c(\boldsymbol{z}_0)$ probes

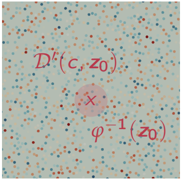

$c = 1.2 * c^\star$

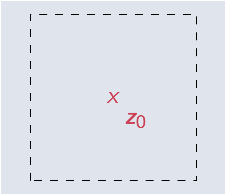

Virtual guide star

Let $\delta > 0$ be a given threshold and c *not too far* from $c^\star$.

- For $\boldsymbol{z} \in D'$, $\mathcal{I}^c(\boldsymbol{z})$ only depends on the scatterers in $\mathcal{D}'_\delta(c, \boldsymbol{z})$

$$\boxed{\mathcal{I}(\boldsymbol{z}, c) = \int_D (n_\varepsilon(\boldsymbol{y}) - n^\star) F^c(\boldsymbol{z}, \boldsymbol{y}) \mathrm{d}\boldsymbol{y} \sim \int_{\mathcal{D}'_\delta(c,\boldsymbol{z})} (n_\varepsilon(\boldsymbol{y}) - n^\star) F^c(\boldsymbol{z}, \boldsymbol{y}) \mathrm{d}\boldsymbol{y}.}$$

- For a fixed $\boldsymbol{y}_0 \in D$, $c \mapsto \mathcal{I}^c(\varphi_c(\boldsymbol{y}_0))$ probes

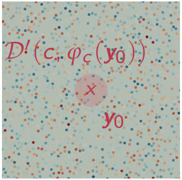

$c = 1.2 * c^\star$

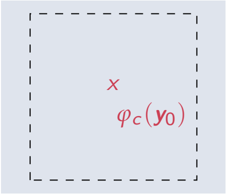

Incoherent estimator

- For $\boldsymbol{y}_0 \in D$, $\mathcal{I}^c(\varphi_c(\boldsymbol{y}_0)) \sim \int_{\mathcal{D}'_\delta(c,\varphi_c(\boldsymbol{y}_0))} (n_\varepsilon(\boldsymbol{y}) - n^\star) F^c(\varphi_c(\boldsymbol{y}_0), \boldsymbol{y}) \mathrm{d}\boldsymbol{y}$.
- If we have access to multiple realizations of $\mathcal{I}^c(\varphi_c(\boldsymbol{y}))$, we compute

$$\boxed{\begin{aligned} \mathbb{E}\left[\left|\mathcal{I}^c(\varphi_c(\boldsymbol{y}_0))\right|^2\right] &\sim \varepsilon^d \|C\|_{L^1(\mathbb{R}^d)} \int_{\mathcal{D}'_\delta(c,\varphi_c(\boldsymbol{y}_0))} |F^c(\varphi_c(\boldsymbol{y}_0), \boldsymbol{y})|^2 \mathrm{d}\boldsymbol{y} \\ &\sim \varepsilon^d \|C\|_{L^1(\mathbb{R}^d)} |\mathcal{D}'_\delta(c, \varphi_c(\boldsymbol{y}_0))| |F^c(\varphi_c(\boldsymbol{y}_0), \boldsymbol{y}_0)|^2 \end{aligned}}$$

where C is the covariance of n, *i.e.* for all $\boldsymbol{x} \in \mathbb{R}^d$

$$\boxed{C(\boldsymbol{x}) := \mathbb{E}[n(\cdot)n(\cdot + \boldsymbol{x})].}$$

- We consider the following incoherent estimator

$$\boxed{\hat{c^\star}^{(1)} := \mathrm{argmax}_c \mathbb{E}\left[\left|\mathcal{I}^c(\varphi_c(\boldsymbol{y}_0))\right|^2\right]}$$

Local stationarity

Note that $\varphi^c(\boldsymbol{y}) = \left(c^2\eta^{\frac{1}{2}}\tilde{y}^{\perp}, c\tilde{y}^{\shortparallel}\right)$ with $\tilde{\boldsymbol{y}} := (\eta^{\frac{1}{2}}\frac{y^{\perp}}{(c^\star)^2}, \frac{y^{\shortparallel}}{c^\star})$.

Proposition : Local stationarity

For $\xi \in \mathbb{R}$, $t > 0$, let $\boldsymbol{z}(c) := (\eta^{\frac{1}{2}}c^2\xi, ct)$.
Then for *a.e.* $\varpi \in \Omega$ and $\boldsymbol{\zeta} \in \mathbb{R}^2$,

$$\mathcal{I}^c(\boldsymbol{z}(c) + \boldsymbol{\zeta}, \varpi) \sim \mathcal{I}^c(\boldsymbol{z}(c), \tau_{\varphi_c^{-1}(\boldsymbol{\zeta})}\varpi)$$

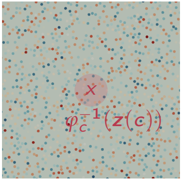

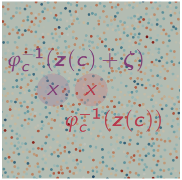

Local stationarity

Note that $\varphi^c(\boldsymbol{y}) = \left(c^2\eta^{\frac{1}{2}}\tilde{y}^{\perp}, c\tilde{y}^{\shortparallel}\right)$ with $\tilde{\boldsymbol{y}} := (\eta^{\frac{1}{2}}\frac{y^{\perp}}{(c^\star)^2}, \frac{y^{\shortparallel}}{c^\star})$.

Proposition : Local stationarity

For $\xi \in \mathbb{R}$, $t > 0$, let $\boldsymbol{z}(c) := (\eta^{\frac{1}{2}}c^2\xi, ct)$.
Then for $a.e.\,\varpi \in \Omega$ and $\boldsymbol{\zeta} \in \mathbb{R}^2$,

$$\mathcal{I}^c(\boldsymbol{z}(c) + \boldsymbol{\zeta}, \varpi) \sim \mathcal{I}^c(\boldsymbol{z}(c), \tau_{\varphi_c^{-1}(\boldsymbol{\zeta})}\varpi)$$

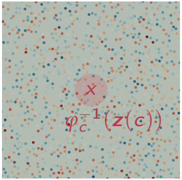

From spatial averaging to ensemble averaging

$$\frac{1}{|B(0,a)|}\int_{B(0,a)} |\mathcal{I}^c(\boldsymbol{z}(c)+\boldsymbol{\zeta})|^2 \,\mathrm{d}\boldsymbol{\zeta} \underset{a \gg \varepsilon}{\sim} \mathbb{E}\left[|\mathcal{I}^c(\boldsymbol{z}(c))|^2\right].$$

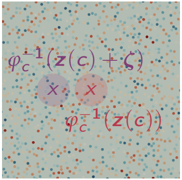

Numerical simulations - Emile Parolin (Alpines, Inria)

· Parameters of the simulation: 166864 scatterers, $\varepsilon = 38.5\mu$m, $\lambda = 0.385$mm, $f = 4$ MHz

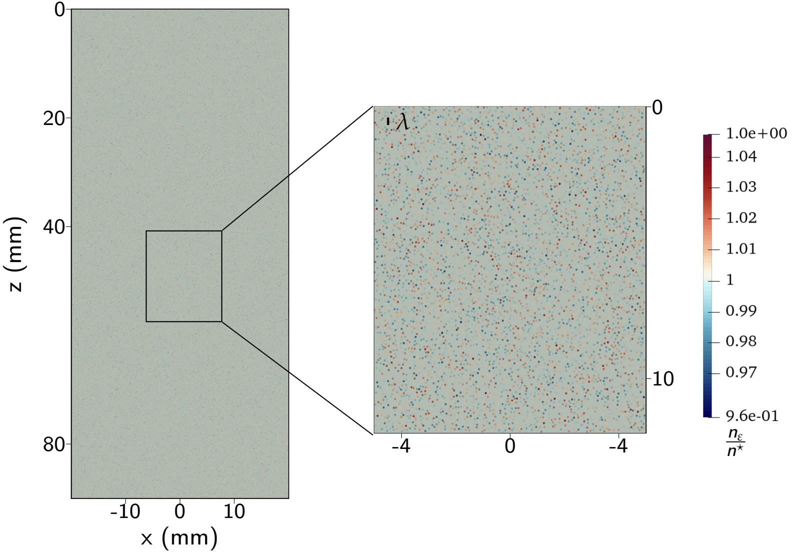

Numerical simulations - Emile Parolin (Alpines, Inria)

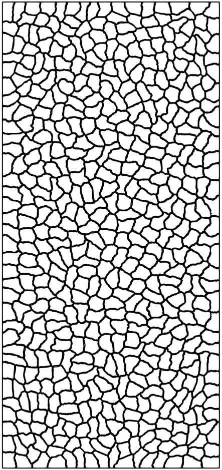

Figure : Partition of the domain

- Parameters of the simulation:
  - Discretisation: 10^8 DOFs (P3),
  - Preconditioner: one-level DD method (ORAS) with 512 subdomains,
  - Solver: 164 GMRES iterations for a 10^{-4} residual tolerance ,
  - Computation time: ~ 5 min on INRIA Paris' supercomputer.

implemented with Freefem++.

Numerical simulations - Emile Parolin (Alpines, Inria)

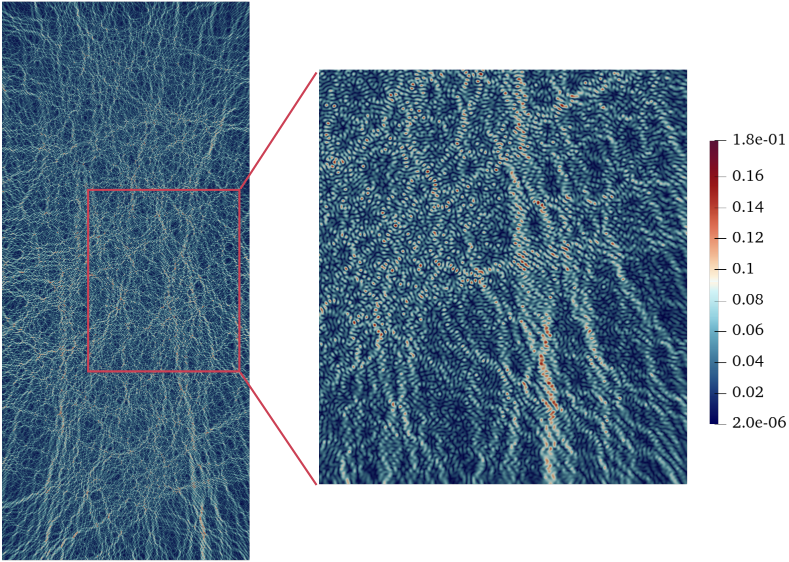

Figure: $|u_\varepsilon^s|$

Numerical simulations

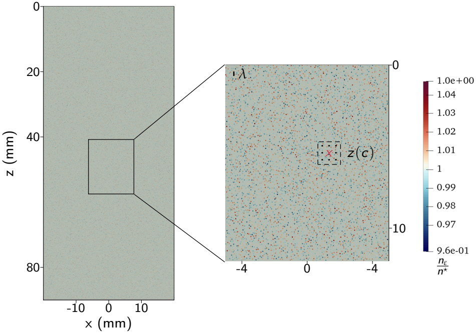

Figure: Speed of sound map

in a random multi-scale medium

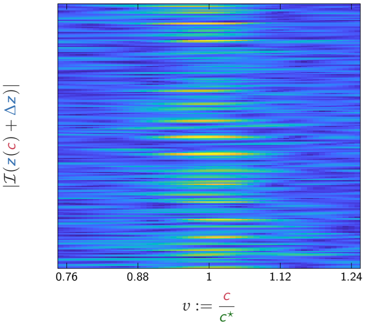

Figure: Plot of $|\mathcal{I}^c(\boldsymbol{z}(c)+\Delta\boldsymbol{z})|$.

Incoherent estimator

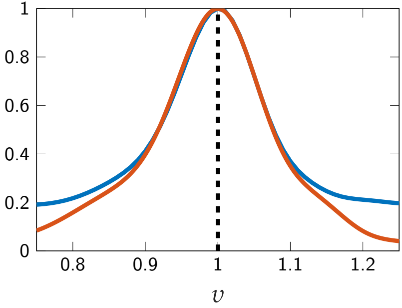

Figure: Simulation (▬) & theoretical (▬) estimators of the speed of sound.

$$\boxed{\hat{c^\star}^{(1)} := \mathrm{argmax}_c \mathbb{E}\left[\left|\mathcal{I}^c(\boldsymbol{z}(c))\right|^2\right]}$$

A better coherent estimator

- Let $\mathcal{K} : L^2((c_{\min}, c_{\max})) \to L^2(\Omega)$ be the kernel operator defined by:

$$\forall f \in L^2((c_{\min}, c_{\max})), \quad [\mathcal{K}f](\varpi) := \int_{c_{\min}}^{c_{\max}} \mathcal{I}^c(\boldsymbol{z}(c), \varpi) f(c) \mathrm{d}c.$$

Estimator via the left singular vector of $\mathcal{K}$

$\mathcal{S} := \mathcal{K}^* \mathcal{K}$ is approximated by:

$$[\mathcal{S}g](c) \sim \varepsilon^d \|C\|_{L^1(\mathbb{R}^d)} \int_{c_{\min}}^{c_{\max}} g(c') \int_{\mathcal{D}_\delta(\boldsymbol{z}(c)) \cap \mathcal{D}_\delta(\boldsymbol{z}(c'))} F^c(\boldsymbol{z}(c), \boldsymbol{y}) F^{c'}(\boldsymbol{z}(c'), \boldsymbol{y}) \mathrm{d}\boldsymbol{y} \mathrm{d}c'.$$

for $g \in L^2((c_{\min}, c_{\max}))$.

The first eigenvector U of $\mathcal{S}$ can be used to recover the speed of sound.

Numerical illustration - $\mathcal{S}$

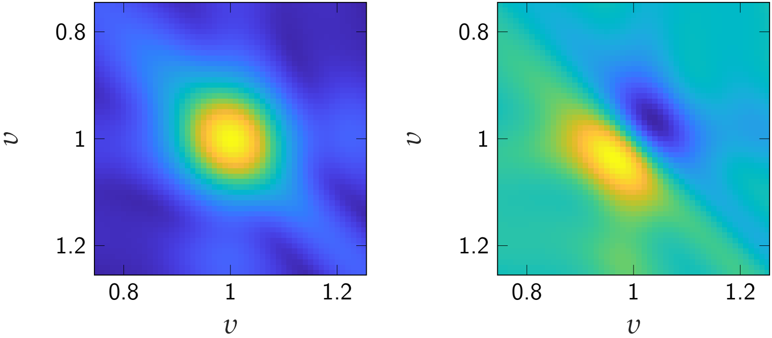

(a) Plot of $|\mathcal{S}|$.

(b) Plot of $\Im[\mathcal{S}]$.

Figure: Modulus and imaginary part of the operator S.

Numerical illustration - a better coherent estimator

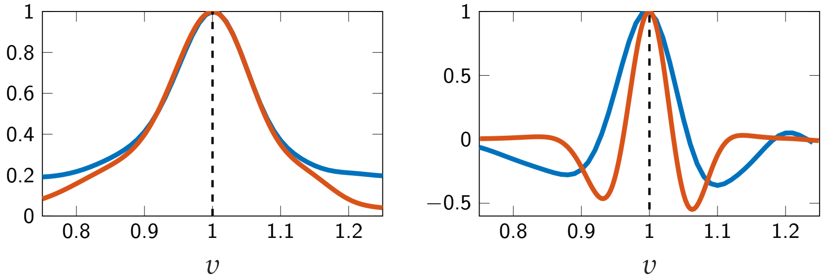

(a) $\hat{c}^{\star(2)} := \operatorname{argmax}_c |U(\boldsymbol{z}(c), c)|$.   (b) $\hat{c}^{\star(3)} := \operatorname{argmax}_c \partial_c \mathrm{Im}[U(\boldsymbol{z}(c), c)]$.

Figure: Simulation (▬) & theoretical (▬) estimators of the speed of sound.

Comparison with the experiment [2]

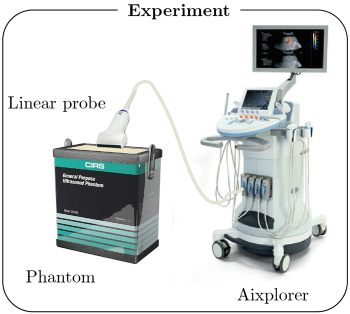

Figure: Experiment done by F. Bureau.

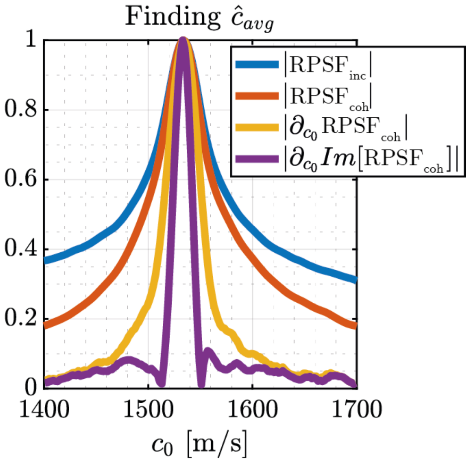

Figure: Experimental estimators [2]

[2] F. Bureau, Multi-dimensional analysis of the reflection matrix for quantitative ultrasound imaging, PhD thesis (2023).

Comparison with the experiment [2]

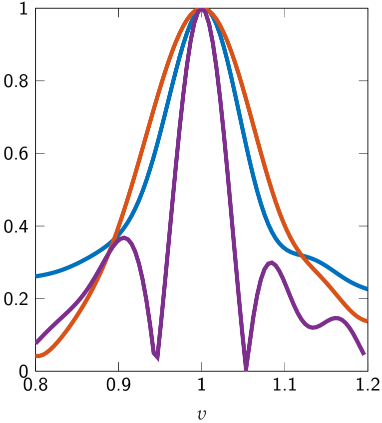

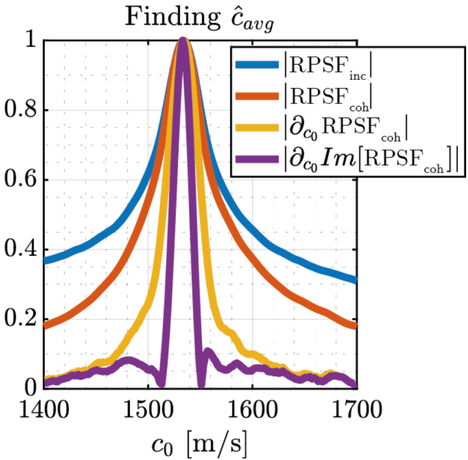

(—) : $\hat{c^\star}^{(1)}$ (—) : $\hat{c^\star}^{(2)}$ (—) : $\hat{c^\star}^{(3)}$

Figure: Experimental estimators [2]

[2] F. Bureau, Multi-dimensional analysis of the reflection matrix for quantitative ultrasound imaging, PhD thesis (2023).

Conclusion and Perspectives

- Conclusion:
  - We developed a new model for wave propagation in random multi-scale media using state of the art homogenization techniques.
  - This model has been used to study the estimators of the propagation speed introduced by Aubry in the context of ultrasound imaging.
- Perspectives:
  - Extend the speed of sound estimation method to
    - more realistic situations starting with media with a slowly varying effective speed of sound,
    - anisotropic media with contrast both in the bulk modulus and density.
  - Characterize the scattered field in polycristalline materials like titanium
  - Construct and analyze a two-level domain decomposition method for wave propagation in anistropic random multi-scale media [5]

[5] E. Parolin, F. Nataf (2024)

Thank you for your attention!